nature communications

Article

https://doi.org/10.1038/s41467-025-60107-7

Linker-free PROTACs efficiently induce the degradation of oncoproteins

Received: 22 September 2024

Accepted: 15 May 2025

Published online: 23 May 2025

Check for updates

Jianchao Zhang[1,9], Congli Chen[2,9], Xiao Chen[1,9], Kefan Liao[1], Fengming Li[3], Xiaoxiao Song[1], Chaowei Liu[1], Ming-Yuan Su[1,4,5,6], Huiyong Sun[7], Tingjun Hou[8], Chris Soon Heng Tan[3], Lijing Fang[2] ✉ & Hai Rao[1,4,6] ✉

Proteolysis-targeting chimeras (PROTACs) present a potentially effective strategy against various diseases via selective proteolysis. How to increase the efficacy of PROTACs remains challenging. Here, we explore the necessity of the linker, which has been deemed as an integral part of heterobifunctional PROTACs. Adopting single amino acid-based degradation signals, we find that the linker is not a required feature of the PROTACs. Notably, the linker-free PROTAC, Pro-BA, exhibits superior efficacy over its linker-bearing counterparts in degrading EML4-ALK and inhibiting lung cancer cell growth, as Pro-BA induces a stronger interaction between the target and the E3 ubiquitin ligase. Pro-BA is a water-soluble, orally administered degrader that significantly inhibits the tumor growth in a xenograft mouse model. The broad applicability of this linker-free PROTAC strategy is further validated through the development of BCR-ABL degrader. Our study introduces a design paradigm for PROTACs, potentially facilitating the advancement of more efficient therapeutic degraders.

Targeted protein degradation (TPD) technology has offered a promising modality to eliminate disease-causing proteins by leveraging the cellular protein degradation machinery. Proteolysis-targeting chimeras (PROTACs) and molecular glues (MGs) represent the most prevalent cutting-edge TPD approaches and have already been adopted in clinical applications[1,2]. Typical PROTACs are assembled in a modular fashion, attaching a ligand for the protein of interest (POI) to an E3 ubiquitin ligase binding moiety through a linker in the middle[1,3]. As a heterobifunctional agent, the PROTAC subjects a desired target to E3-mediated ubiquitylation and subsequent proteasomal degradation. The linker portion is deemed necessary and likely serves as a critical spacer that promotes the productive reaction. This modularity allows for flexible and tailored design, though it often results in a larger molecular weight compared to traditional small-molecule drugs. In contrast, MG degraders tend to be much smaller, with molecular weights under 500 Da, adhering to Lipinski's rule of five for drug-like properties[2,4]. Nevertheless, the discovery of MGs often relies on serendipity and lacks well-established design frameworks[5,6]. Thus, it remains a major challenge in the TPD field to establish rational and modular design principles for small yet efficient degraders.

While most of the PROTACs (~90%) have employed the degradation signals for CRBN or VHL E3 ubiquitin ligases, we have developed a series

[1]Department of Biochemistry, School of Medicine, Southern University of Science and Technology, Shenzhen, China. [2]Guangdong Key Laboratory of Nanomedicine, CAS-HK Joint Lab of Biomaterials, Key Laboratory of Biomedical Imaging Science and System, Chinese Academy of Sciences, State Key Laboratory of Biomedical Imaging Science and System, Institute of Biomedicine and Biotechnology, Shenzhen Institute of Advanced Technology (SIAT), Chinese Academy of Sciences, Shenzhen, China. [3]Department of Chemistry, Southern University of Science and Technology, Shenzhen, China. [4]Key University Laboratory of Metabolism and Health of Guangdong, Southern University of Science and Technology, Shenzhen, China. [5]Institute for Biological Electron Microscopy, Southern University of Science and Technology, Shenzhen, China. [6]SUSTech Homeostatic Medicine Institute, School of Medicine, Southern University of Science and Technology, Shenzhen, China. [7]Department of Medicinal Chemistry, China Pharmaceutical University, Nanjing, Jiangsu, China. [8]College of Pharmaceutical Sciences, Zhejiang University, Hangzhou, Zhejiang, China. [9]These authors contributed equally: Jianchao Zhang, Congli Chen, Xiao Chen. ✉e-mail: lj.fang@siat.ac.cn; raoh@sustech.edu.cn

of single amino acid-based PROTACs termed AATac[7–10]. The first genetically defined ubiquitin-mediated proteolytic pathway is the N-end rule pathway, which connects the protein's half-life to the specific amino acid residue at its N-terminus (i.e., N-degron)[11–14]. The UBR family E3 ubiquitin ligases (e.g., UBR1, UBR2, UBR4, and UBR5) recognize basic amino acids (i.e., Arg, His, Lys) and bulky hydrophobic residues (i.e., Leu, Ile, Phe, Trp, Tyr)[11]. The CTLH E3 ligase complex can select the substrates bearing the N-terminal residues, including Pro, Val, and Phe, for ubiquitylation and degradation[13,15,16]. ZYG11B and ZER1, acting as adaptors for the Cullin 2-RING E3 ubiquitin ligase (CRL2), recognize the N-terminal Gly, Cys, Ala, Ser, and Thr[14,17]. Utilizing the N-end rule pathway, these AATacs efficiently trigger targeted protein degradation and suppress cancer cell growth in vitro and in vivo[8–10].

Whereas the functions of the ligands for the target protein and E3 ligase in the PROTAC development are clearly defined, the linkers appear to serve largely as an essential spacer in the early pioneering PROTAC research and remain an integral part of the PROTAC design[18–21]. Nevertheless, the effective type and length of the linker are hard to predict and are often adopted through trial and error, presenting significant costs in terms of time, money, effort, and potentially technical hurdles. The inclusion of a linker also increases the PROTAC size, often pushing it over 500 Da and violating Lipinski's rule of five, which is a major concern for drug efficacy. Is a linker always needed for PROTACs? Developing a strategy that simplifies or even bypasses the laborious linker optimization process in PROTAC design would be highly desirable. Recent studies have explored the application of chemical moieties that can covalently bind to E3 ligases, in combination with various ligands of POIs, enabling the degradation of their targets without the necessity of a linker[22–29]. As several of our amino acid-based PROTACs work fine with short PEG linkers, we sought to further delineate the requirement of linker for AATacs.

Herein, we develop linker-free PROTACs by directly coupling an N-degron to the ligands of various oncoproteins, including EML4-ALK and BCR-ABL. We find that these minimal AATacs can effectively induce the degradation of various oncogenic kinases. In our in-depth analysis, the linker-free Pro-BA molecule demonstrates superior performance over Pro-PEG3-BA, which bears three units of PEG, in substrate binding, ubiquitylation and degradation, cell growth inhibition, and anti-tumor efficacy. By varying the N-degrons coupled with different ligands, we have developed small (~500 Da), versatile degraders with broad applicability, making this a promising strategy for diverse therapeutic targets.

Results

Design and biological evaluation of the linker-free PROTACs in non-small cell lung cancer (NSCLC) cells

We have previously demonstrated that distinct N-degrons attached to the ALK ligand Brigatinib analog (BA) with three units of PEG as the linker efficiently induced EML4-ALK degradation[10]. To explore the necessity of a linker in AATacs, we directly conjugated these N-degrons —Pro, Gly, and Arg—with BA, designing three linker-free PROTACs: Pro-BA, Gly-BA, and Arg-BA (Fig. 1A). Whereas Pro-BA and Gly-BA individually resulted in a significant reduction of EML4-ALK protein levels in H3122 cells starting at 100 nM (Fig. 1B), Arg-BA induced a decrease in EML4-ALK protein levels at 10 μM with no notable effect below 500 nM (Fig. 1B and Supplementary Fig. 1A). Therefore, we selected the more effective compounds, Pro-BA and Gly-BA, for further investigation. By refining the concentration gradients, we determined that Pro-BA had a DC_{50} of 74 nM and achieved an 82% reduction at 500 nM, whereas Gly-BA had a DC_{50} of 142 nM and attained a 76% reduction at 500 nM (Fig. 1C, D and Supplementary Fig. 1B). The CCK-8 assay was then carried out to evaluate the growth inhibition of these linker-free AATacs in H3122 cells. The IC_{50} value for Pro-BA was 34 nM, whereas Gly-BA had an IC_{50} value of 69 nM (Fig. 1D, E). Compared to our previous study[10] and the data below (Fig. 2), both linker-free Pro-BA and Gly-BA are more potent than their linker-bearing counterparts Pro-PEG3-BA (DC_{50}: 416 nM, IC_{50}: 156 nM) and Gly-PEG3-BA (DC_{50}: 500 nM, IC_{50}: 840 nM), respectively.

We subsequently assessed the temporal dynamics of EML4-ALK degradation induced by linker-free AATacs. H3122 cells were exposed to Pro-BA or Gly-BA at 250 nM for varying durations. Pro-BA led to a decrease in EML4-ALK protein levels at 3 h, while Gly-BA initiated a reduction in EML4-ALK protein levels at around 0.5 h (Fig. 1F and Supplementary Fig. 1C). Pro-BA exhibited a $T_{1/2}$ (the time for 50% disappearance of protein) of 8 h, which was slightly shorter than that of Gly-BA, with a $T_{1/2}$ of 10 h (Fig. 1F), suggesting that although Gly-BA initiates degradation more quickly, Pro-BA may achieve a better overall clearance of the protein. These findings underscore the superior potency of Pro-BA compared to Gly-BA, leading us to prioritize Pro-BA for further detailed analysis.

We next evaluated the activity of Pro-BA in BaF3-EML4-ALK cells, a well-established model in kinase drug discovery. We found that it efficiently induced the degradation of EML4-ALK, with a DC_{50} of 125 nM (Supplementary Fig. 2A). The degradation of EML4-ALK was initiated as early as 0.5 h, with a $T_{1/2}$ of ~2 h (Supplementary Fig. 2B). In contrast, the unmodified ALK inhibitor Brigatinib had no effect on the levels of EML4-ALK at the corresponding time points (Supplementary Fig. 2C). Furthermore, the CCK8 assay showed that Pro-BA inhibited cell proliferation after 3 h post-treatment (Supplementary Fig. 2D), whereas Brigatinib inhibited cell proliferation as early as 0.5 h post-treatment (Supplementary Fig. 2E). The data illustrate that Pro-BA-driven EML4-ALK degradation and antiproliferation largely coincide in their timing. Flow cytometry analysis further revealed that Pro-BA increases the fraction of both early and late apoptotic cells after 3 h, with no significant change observed within 1 h (Supplementary Fig. 2F, G). Collectively, the data demonstrate that Pro-BA-induced degradation of EML4-ALK and cell death occur within a comparable time frame, with degradation initiating slightly earlier. However, this time difference is minimal, suggesting that both processes largely overlap in their temporal progression.

We further evaluated the effects of Pro-BA on wild-type ALK in neuroblastoma SK-N-BE(2) cells, where ALK is localized on the cell membrane. Our results demonstrated that Pro-BA induced ALK degradation with a DC_{50} value of 2.1 μM (Supplementary Fig. 3A). Notably, this DC_{50} is ~29 times higher than that for EML4-ALK degradation in H3122 cells, indicating a stronger selectivity for EML4-ALK over ALK.

To explore the broader impact of Pro-BA on the cellular proteome, we used quantitative proteomics to analyze global protein abundance in H3122 cells treated with DMSO or 500 nM Pro-BA for 12 h. EML4-ALK was one of the primary downregulated proteins following Pro-BA treatment, with a substantial reduction of over 40-fold, along with a decrease in its downstream target, RRM2[30] (Fig. 1G). These results underscore the relatively high selectivity of Pro-BA in targeting EML4-ALK for degradation.

Pro-BA displays superior performance compared to their linker-bearing Pro-based PROTACs in vitro

In our previous study of AATacs bearing 1-4 units of PEG linker, we found Pro-PEG3-BA was the most potent in triggering EML4-ALK degradation[10]. Next, we directly compared the efficacy of linker-free Pro-BA with Pro-based AATacs featuring varying numbers of PEG units. H3122 cells were treated with Pro-BA, Pro-PEG1-BA, and Pro-PEG3-BA at 100 nM for 48 h. Pro-BA led to a noticeable reduction in EML4-ALK levels at 100 nM (Fig. 2A). In contrast, Pro-PEG1-BA and Pro-PEG3-BA did not overtly affect EML4-ALK protein levels at the same concentration (Fig. 2A). The CCK-8 assay revealed that Pro-BA was more potent in blocking cell growth than Pro-PEG1-BA and Pro-PEG3-BA (Fig. 2B, C). We also observed that Pro-BA had a lower DC_{50} and a higher D_{max} in comparison to Pro-PEG1-BA and Pro-PEG3-BA (Fig. 2C and Supplementary Fig. 3B).

https://doi.org/10.1038/s41467-025-60107-7

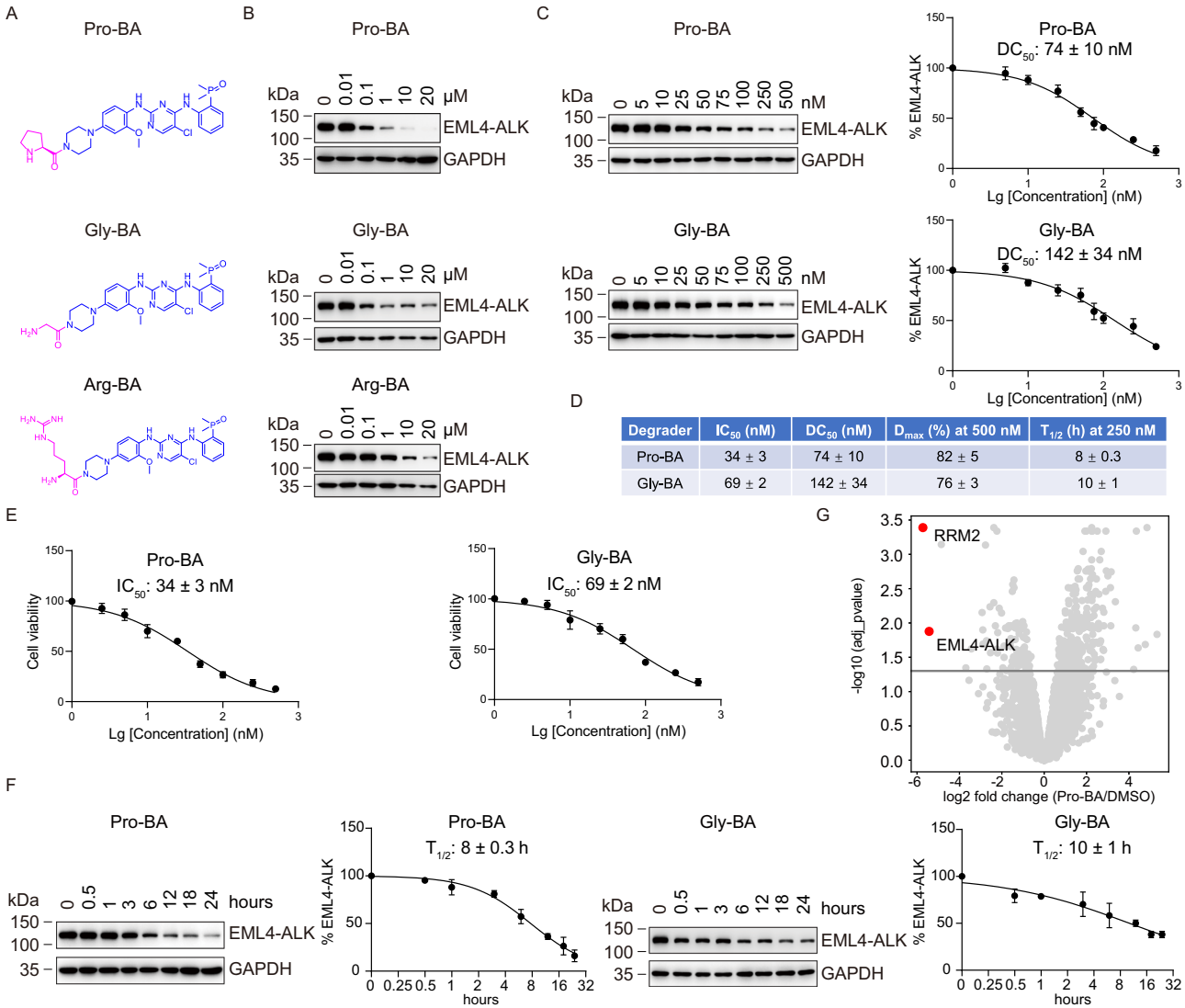

Fig. 1 | Linker-free AATacs mediate the degradation of EML4-ALK. A The schematic designs of Pro-BA, Gly-BA and Arg-BA. **B** H3122 cells were exposed to Pro-BA, Gly-BA, or Arg-BA at the specified concentrations for 48 h, and protein levels of EML4-ALK and GAPDH were assessed by immunoblotting. **C** H3122 cells were separately treated with Pro-BA or Gly-BA at the indicated concentration for 24 h, followed by immunoblot analysis of EML4-ALK and GAPDH protein expression (left panel). The plots were utilized to determine the half-maximal degradation concentration (DC_{50}) values by quantifying EML4-ALK protein levels (right panel). **D** Summary of DC_{50} values—defined as the drug concentration resulting in 50% protein degradation, D_{max} values—defined as the maximum degradation percentage relative to control, IC_{50} values—defined as the half maximal inhibitory concentration, and $T_{1/2}$ values- defined as the time leading to 50% protein degradation for Pro-BA and Gly-BA. **E** H3122 cell viability was determined utilizing CCK-8 assays after 48 h of treatment with different concentrations of Pro-BA and Gly-BA. **F** Immunoblot analysis was performed on H3122 cells treated with 250 nM Pro-BA or Gly-BA for different time intervals (left panel). The curves were analyzed to calculate $T_{1/2}$ values based on the quantification of EML4-ALK protein levels (right panel). **G** Quantitative proteomics analysis in H3122 cells after treatment with DMSO or 500 nM Pro-BA for 12 h. Data are presented as the log2 fold change (FC) in protein abundance (*x*-axis) versus the -log10 adjusted *p* value (*y*-axis) for each protein, derived from quadruplicate experiments. Two-sided moderated *t*-test *p* values were calculated using the LIMMA package, and the horizontal line represents an adjusted *p* value threshold of 0.05. For (**C**), (**E**), (**F**), the data are shown as mean ± SD derived from three independent experiments. Source data are provided as a Source Data file.

We further compared the effects of Pro-BA, Pro-PEG1-BA, and Pro-PEG3-BA on cell cycle progression and apoptosis. Flow cytometry revealed that Pro-BA induced a higher proportion of cells in the G1 phase and a lower proportion in the S and G2 phases compared to Pro-PEG1-BA and Pro-PEG3-BA, which showed a milder effect on cell cycle distribution after 24 h of treatment at 500 nM in H3122 cells (Fig. 2D, E). Additionally, Pro-BA led to a marked elevation in the percentage of early and late apoptotic cells, whereas Pro-PEG1-BA and Pro-PEG3-BA induced a comparatively lower apoptotic response under the same treatment conditions (500 nM for 24 h in H3122 cells) (Fig. 2F, G).

Next, we measured the solubility of Pro-BA and Pro-PEG3-BA in water and found that Pro-BA exhibited higher solubility (1.8×10^6 μM) compared to Pro-PEG3-BA (8.6×10^5 μM). Additionally, we assessed their cell membrane permeability. The data revealed that the intracellular concentration of Pro-BA was ~1.5 times higher than that of Pro-PEG3-BA, suggesting superior cellular uptake of Pro-BA (Fig. 2H). Taken together, these findings indicate the potential of Pro-BA to improve bioavailability and therapeutic efficacy.

Pro-BA exhibits better anti-tumor effects compared to Pro-PEG3-BA in vivo

To further evaluate the in vivo anti-tumor effects of Pro-BA versus Pro-PEG3-BA and the FDA-approved ALK inhibitor Brigatinib, we established a xenograft tumor model by subcutaneously inoculating H3122

https://doi.org/10.1038/s41467-025-60107-7

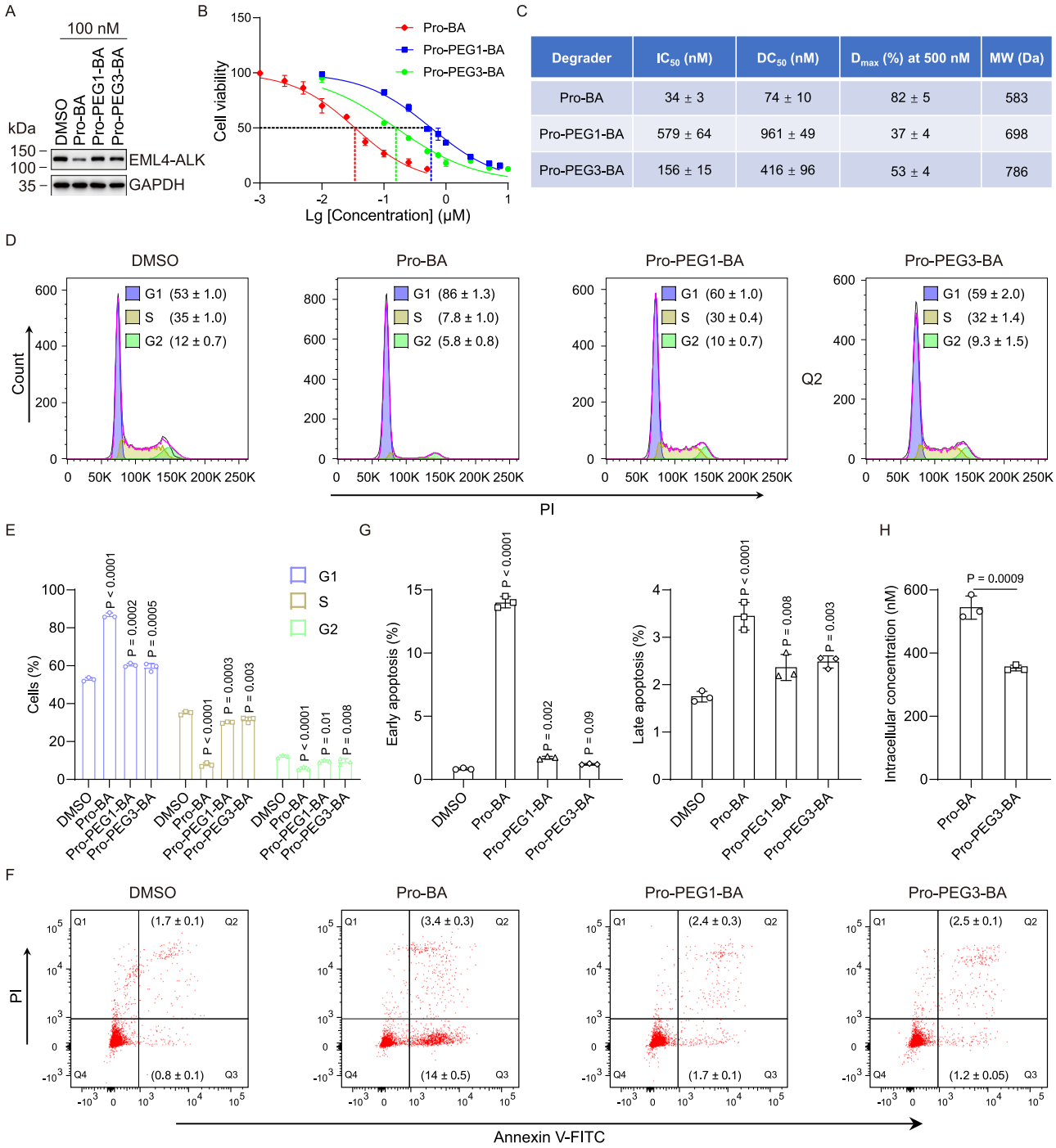

Degrader	IC_{50} (nM)	DC_{50} (nM)	D_{max} (%) at 500 nM	MW (Da)
Pro-BA	34 ± 3	74 ± 10	82 ± 5	583
Pro-PEG1-BA	579 ± 64	961 ± 49	37 ± 4	698
Pro-PEG3-BA	156 ± 15	416 ± 96	53 ± 4	786

Fig. 2 | Linker-free Pro-BA outperforms the linker-containing degraders in vitro. A H3122 cells were incubated with Pro-BA, Pro-PEG1-BA and Pro-PEG3-BA separately at 100 nM for 48 h. The expression levels of EML4-ALK and GAPDH were assessed by immunoblotting. **B** H3122 cell viability was measured via CCK-8 assays following a 48-hour exposure to Pro-BA, Pro-PEG1-BA, and Pro-PEG3-BA at various concentrations. Data is represented as mean ± SD of three independent experiments. **C** Summary of DC_{50}, D_{max}, IC_{50} values, and molecular weight (MW) for the indicated compounds. **D** H3122 cells were exposed to Pro-BA, Pro-PEG1-BA, or Pro-PEG3-BA at 500 nM for 24 h, and cell cycle distribution was assessed using flow cytometry. **E** The bar graph illustrates the percentage of H3122 cells in the G1, S, and G2 phases as shown in (**D**). **F** H3122 cells were treated with Pro-BA, Pro-PEG1-BA or Pro-PEG3-BA at 500 nM for 24 hours, and apoptosis was assessed using flow cytometry. **G** The bar graph shows the percentages of early (left) and late (right) apoptotic cells, as indicated by the Q3 and Q2 quadrants in (**F**), respectively. **H** H3122 cells were treated with 5 μM Pro-BA or Pro-PEG3-BA for 5 h. UHPLC-MS/MS analysis of intracellular amounts of Pro-BA and Pro-PEG3-BA per 5×10^6 cells. Data are presented as mean ± SD from three independent experiments, two-tailed Student's *t*-test. For (**E**), (**G**), data are presented as the mean ± SD ($n = 3$ independent experiments). Statistical analysis was performed using one-way ANOVA followed by Fisher's LSD test (two-tailed). The gating strategies for flow cytometry analysis are shown in Supplementary Fig. 8. Source data are provided as a Source Data file.

cells into the right flanks of female nude mice. Once the tumors reached a palpable size of around 45 mm^3, the H3122 tumor-bearing mice were randomly assigned to four groups and administered with vehicle, Brigatinib, Pro-PEG3-BA, and Pro-BA at a dosage of 10 mg/kg via intraperitoneal (I.P.) injection every other day for a total of 8 doses. The day after the final treatment, the tumors were then surgically removed and photographed (Fig. 3A). The results showed that Pro-BA was the most effective, among the three compounds, in reducing

https://doi.org/10.1038/s41467-025-60107-7

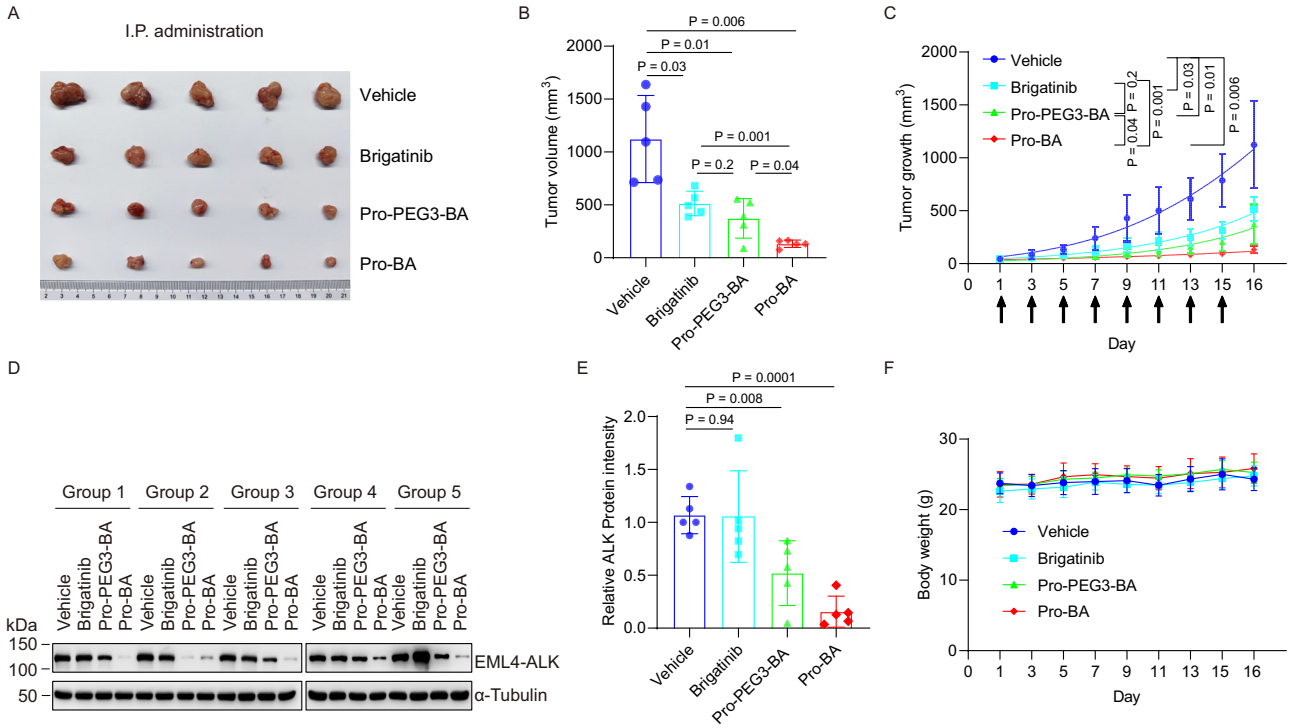

Fig. 3 | Pro-BA shows enhanced antitumor activity compared to the corresponding degraders with linkers in vivo. A H3122 cells were grafted into the right flank of 4-week-old female nude mice. The mice were treated with vehicle, Brigatinib, Pro-PEG3-BA, or Pro-BA at dose of 10 mg/kg, prepared in a solution of 90% corn oil + 10% DMSO via I.P. route every other day for a total of 8 administrations. Tumors were harvested from each group and photographed. **B** The bar graphs represent the mean ± SD of the primary tumor volumes of mice in (**A**). **C** The graph depicts the mean tumor growth of mice in (**A**), with treatment intervals marked by black arrows. **D** Analysis of EML4-ALK protein levels in tumor samples from (**A**) using immunoblotting. **E** Quantitative analysis of the Western blot results presented in (**D**). Data are presented as the mean ± SD ($n = 5$ mice per group). Statistical analysis was performed using one-way ANOVA followed by Fisher's LSD test (two-tailed) for pairwise comparisons. **F** The graph illustrates the average body weight of mice receiving I.P. administration as described in (**C**). For (**B**), (**C**) data are presented as the mean ± SD ($n = 5$ mice per group). Statistical analysis was performed using Brown-Forsythe and Welch ANOVA followed by Welch's t-tests (two-tailed) due to unequal variances ($p < 0.05$). Source data are provided as a Source Data file.

tumor size and inhibiting tumor growth (Fig. 3B, C). Pro-BA also led to a more consistent and pronounced decrease in EML4-ALK protein levels in tumors compared to Pro-PEG3-BA, whereas the ALK kinase inhibitor Brigatinib failed to reduce EML4-ALK protein levels in tumors (Fig. 3D, E). Importantly, none of the treatments caused significant variations in the mice body weight, indicating that the drugs were well tolerated and not overtly toxic in mice (Fig. 3F).

Pro-BA induces the degradation of EML4-ALK through the ubiquitin-proteasome system

The proteasome and the lysosome are two major proteolytic systems in eukaryotic cells. To elucidate which system is responsible for the Pro-BA-triggered EML4-ALK degradation, we exposed Pro-BA-treated H3122 cells to either the proteasome inhibitor MG132 or the lysosome inhibitor chloroquine (CQ). We found that MG132, but not CQ, impeded Pro-BA-induced degradation of EML4-ALK, indicating the involvement of the proteasome pathway (Fig. 4A and Supplementary Fig. 4A). We also assessed the degradation kinetics of EML4-ALK in the presence or absence of Pro-BA treatment. H3122 cells were incubated with cycloheximide (CHX) to halt protein synthesis, and the remaining EML4-ALK protein levels were monitored at various intervals. EML4-ALK protein levels diminished rapidly in Pro-BA-treated cells, but remained at its levels in the DMSO-treated control cells (Fig. 4B and Supplementary Fig. 4B). The turnover of EML4-ALK induced by Pro-BA was hindered by MG132 (Fig. 4B and Supplementary Fig. 4B), supporting the requirement of the proteasome for effective substrate breakdown. The Pro-BA-driven decrease in EML4-ALK was attenuated by excess BA in the competition assay, highlighting the critical role of EML4-ALK and Pro-BA binding for effective degradation (Fig. 4C and Supplementary Fig. 4C).

An E3 ubiquitin ligase is often required to select substrates for ubiquitin decoration, a prerequisite for the proteasome engagement. GID4, serving as the substrate receptor for the CTLH E3 ligase complex, is responsible for recognizing substrates featuring an N-terminal proline[15]. To evaluate the involvement of GID4 in Pro-BA-triggered EML4-ALK turnover, we generated GID4 knockout H3122 cells using CRISPR/Cas9. GID4 depletion largely prevented the Pro-BA-mediated reduction in EML4-ALK levels (Fig. 4D), whereas it had no impact on the degradation of EML4-ALK mediated by Arg-BA or Gly-BA (Supplementary Fig. 4D, E). The degrader-induced proximity between the target and E3 ligase is fundamental for enabling ubiquitin transfer and the subsequent degradation of the target. We then performed co-immunoprecipitation assays to investigate if Pro-BA facilitates the interaction between the target protein EML4-ALK and the E3 ligase GID4. The results showed that the presence of Pro-BA is necessary for the association between EML4-ALK and GID4 (Fig. 4E). Subsequently, we assessed the Pro-BA-induced ubiquitylation of EML4-ALK. We only detected ubiquitylated EML4-ALK species in the Pro-BA–treated cells (Fig. 4F). These data suggest that Pro-BA introduced a new interaction between EML4-ALK and GID4 and subsequently promoted EML4-ALK ubiquitylation.

Next, we probed the mechanistic basis underlying the differences between the linker-free Pro-BA and the linker-bearing Pro-PEG3-BA using various biochemical assays. We first assessed the binding affinities of Pro-BA and Pro-PEG3-BA to ALK in vitro using isothermal titration calorimetry (ITC). The results revealed that Pro-BA and Pro-PEG3-BA bind to purified ALK with dissociation constants of 144 nM and 387 nM, respectively, indicating that Pro-BA exhibits stronger binding affinity to ALK than Pro-PEG3-BA (Fig. 4G).

https://doi.org/10.1038/s41467-025-60107-7

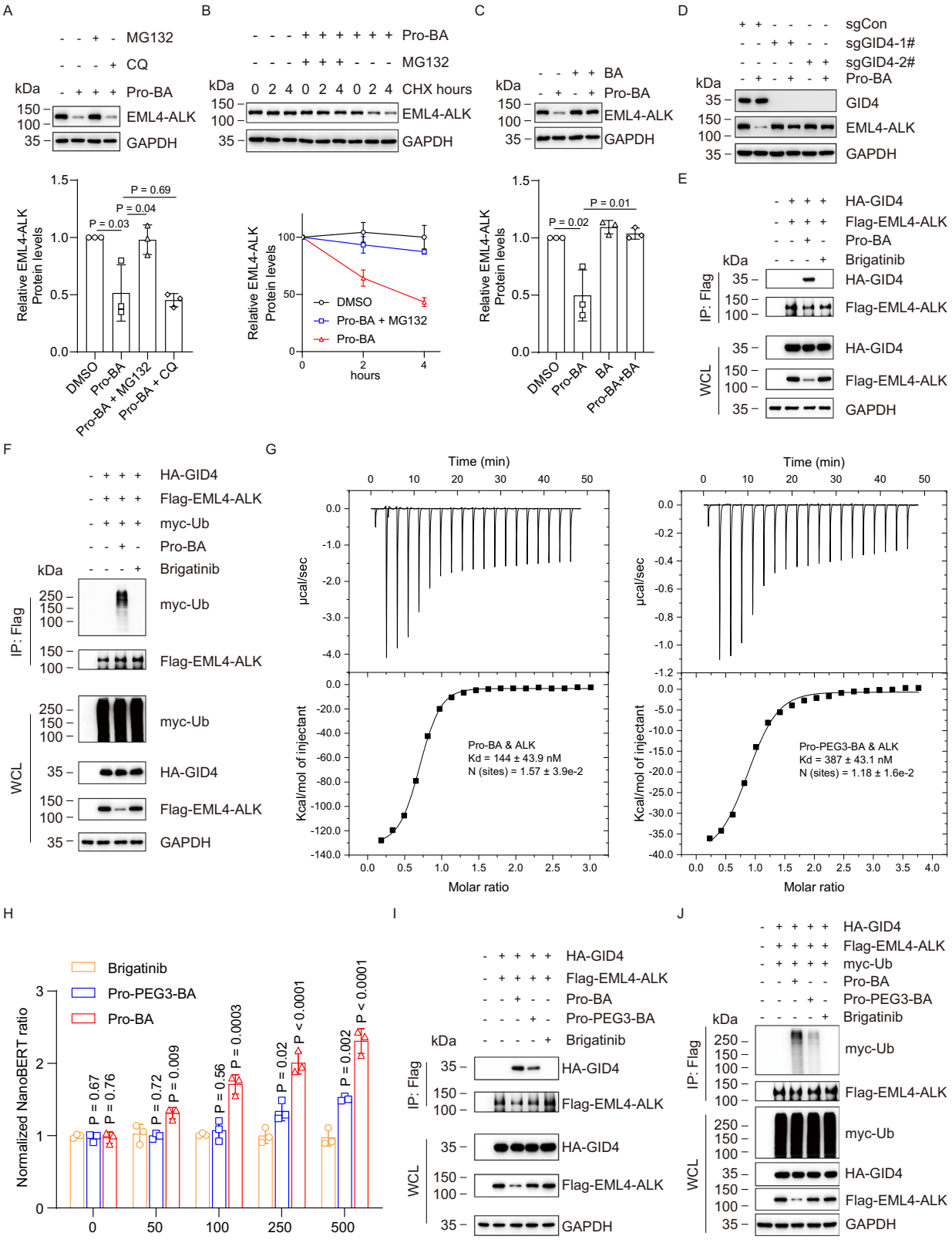

Previous studies have shown a positive correlation between the strength of PROTAC-mediated E3-substrate interaction and the effectiveness of target protein ubiquitylation and degradation[31–33]. To assess the extent of ternary complex formation involving GID4, ALK, and Pro-BA versus Pro-PEG3-BA in living cells, we carried out a NanoBRET assay. Both compounds increased the BRET signal in a dose-dependent manner, but the Pro-BA treatment resulted in a significantly higher BRET signal between GID4 and ALK compared to Pro-PEG3-BA, whereas Brigatinib did not induce any BRET signal, even with increasing concentrations (Fig. 4H). Moreover, we performed co-immunoprecipitation experiments to assess the GID4 and EML4-ALK interaction after treatment with DMSO, Brigatinib, Pro-BA, or Pro-PEG3-BA. We observed that Flag-tagged EML4-ALK co-immunoprecipitated a larger amount of HA-GID4 in the cells

Fig. 4 | Pro-BA facilitates EML4-ALK degradation through the ubiquitin-proteasome system. A H3122 cells were treated with Pro-BA alone or in combination with MG132 (10 μM) or CQ (25 μM), for 6 h. The protein levels of EML4-ALK and GAPDH were subsequently assessed by immunoblotting (upper panel). The bar graph presents a quantitative analysis of EML4-ALK protein levels derived from three independent replicates shown in Fig. 4A and Supplementary Fig. 4A (lower panel). **B** H3122 cells were treated with cycloheximide (CHX) alone, or in combination with Pro-BA, or with both Pro-BA (100 nM) and MG132 (10 μM) for different time intervals, followed by immunoblotting to measure EML4-ALK and GAPDH expression (upper panel). Quantitative analysis of the Western blot results for EML4-ALK from three separate repeats is presented in Fig. 4B and Supplementary Fig. 4B (lower panel). **C** Immunoblot analysis was conducted on H3122 cells pre-treated with BA (10 μM) for 2 h and then incubated with Pro-BA (100 nM) for 12 h to assess the expression of specific proteins (upper panel). The bar graph presents a quantitative analysis of EML4-ALK protein levels derived from three independent experiments shown in Fig. 4C and Supplementary Fig. 4C (lower panel). **D** H3122 cells with stable expression of the indicated sgRNA were exposed to either DMSO or Pro-BA for 24 h, and the levels of the indicated protein were assessed by immunoblotting. **E** HEK293T cells co-expressing HA-GID4 and Flag-EML4-ALK were treated with DMSO, Pro-BA (500 nM), or Brigatinib (500 nM) for 24 h. The cells were then subjected to immunoprecipitation using anti-FLAG® M2 Magnetic Beads, followed by immunoblotting with the specified antibodies. **F** HEK293T cells co-expressing HA-GID4, Flag-EML4-ALK, and myc-Ub were incubated with DMSO, Pro-BA (500 nM), or Brigatinib (500 nM) for 24 h, then treated with MG132 (10 μM) for 4 h. Ubiquitylation of Flag-EML4-ALK was analyzed by denaturing immunoprecipitation (IP) with an anti-myc-tag antibody. **G** ITC measurement of the affinity of Pro-BA (left) and Pro-PEG3-BA (right) with ALK (1094-1400 aa). **H** HEK293T cells co-transfected with pHTN-GID4 and pNLF1-N-ALK were exposed to Brigatinib, Pro-BA, or Pro-PEG3-BA at the indicated concentration for 6 h. Data represented as normalized NanoBRET ratio. Data are presented as the mean ± SD ($n = 3$ independent experiments). Statistical analysis was performed using one-way ANOVA followed by Fisher's LSD test (two-tailed) for pairwise comparisons. **I** HEK293T cells coexpressing HA-GID4 and Flag-EML4-ALK were incubated with DMSO, Pro-BA (500 nM), Pro-PEG3-BA (500 nM), or Brigatinib (500 nM) for 24 h, respectively. After immunoprecipitation with anti-FLAG® M2 Magnetic Beads, followed by immunoblotting with various antibodies indicated. **J** HEK293T cells coexpressing HA-GID4, Flag-EML4-ALK, and myc-Ub were treated with DMSO, Pro-BA (500 nM), Pro-PEG-BA (500 nM), or Brigatinib (500 nM) for 24 h, followed by the addition of MG132 (10 μM) for 4 h. Ubiquitination of Flag-EML4-ALK was examined by denaturing immunoprecipitation (IP) with anti-myc-tag antibody. For (**A**–**C**), data are shown as the mean ± SD ($n = 3$ independent experiments), two-tailed Student's *t*-test. Source data are provided as a Source Data file.

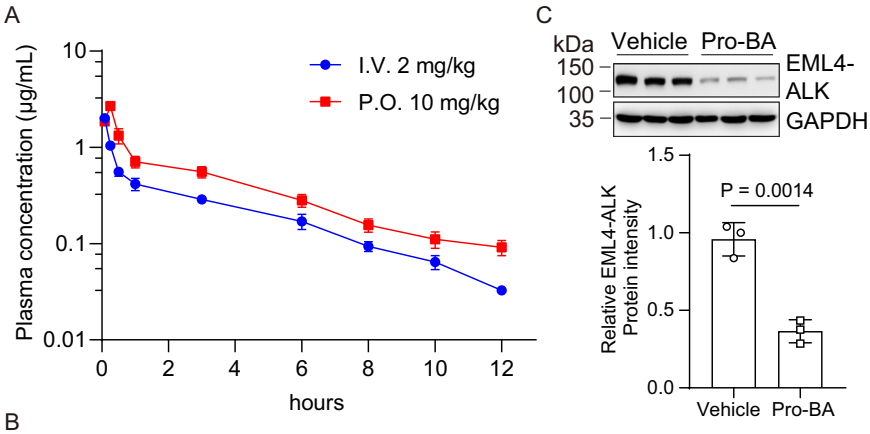

B

PK Parameters of Pro-BA in mice (n = 3)								
Administration	T_{max} (h)	$T_{1/2}$ (h)	C_{max} (μg/mL)	$AUC_{0\text{-}t}$ (h*μg/mL)	Vd (L/kg)	$CL_{\_F\_obs}$ (mL/h/kg)	MRT_{last} (h)	F (P.O.) %
I.V. (2 mg/kg)	0.083	3.0 ± 0.3	2.0 ± 0.1	2.8 ± 0.3	3.0 ± 0.5	681 ± 54	3.1 ± 0.1	
P.O. (10 mg/kg)	0.25	3.4 ± 0.1	2.7 ± 0.2	4.9 ± 0.7	9.4 ± 1.0	1892 ± 253	3.2 ± 0.04	35 ± 5

Fig. 5 | In vivo PK and PD studies of Pro-BA. A Pro-BA was administered to mice at a dose of 2 mg/kg in ddH_2O via I.V. injection and 10 mg/kg in ddH_2O via P.O. route, respectively. Plasma drug concentrations were assessed utilizing HPLC. Data are presented as the mean ± SD ($n = 3$ mice per group). **B** PK parameters of Pro-BA following a single dose via I.V. injection (2 mg/kg) and P.O. route (10 mg/kg). **C** H3122 tumor-bearing nude mice received either vehicle (ddH_2O) or Pro-BA (10 mg/kg in ddH_2O) via P.O. route. Tumor tissues were collected and analyzed by immunoblotting to detect indicated proteins after 48 h of treatment (upper panel). The corresponding quantification of protein levels from the western blot data is provided (lower panel). Data are presented as the mean ± SD (n = 3 mice per group), two-tailed Student's *t*-test. Source data are provided as a Source Data file.

treated with Pro-BA than those treated with Pro-PEG3-BA (Fig. 4I). We also compared the impact of Pro-BA and Pro-PEG3-BA on EML4-ALK ubiquitylation. We found that Pro-BA promoted a higher level of EML4-ALK ubiquitylation than Pro-PEG3-BA (Fig. 4J). Combined, these data suggest that linker-free Pro-BA promotes a more robust interaction between the target protein and E3 ligase, which in turn boosts substrate ubiquitylation and degradation.

Pro-BA effectively suppresses tumor growth through oral administration in vivo

Oral administration offers a convenient and patient-friendly route of drug delivery. To evaluate the potential of Pro-BA as an orally administered antitumor therapy, we first carried out pharmacokinetic (PK) studies in mice to investigate its oral bioavailability. The compound displayed a favorable PK profile following oral administration (P.O.) in mice, characterized by a reasonable half-life of 3.4 h ($T_{1/2}$), a good volume of distribution at steady state (Vd = 9.4 L/kg), a moderate clearance (CL = 1892 mL/h/kg), a high oral plasma exposure with a maximum plasma concentration (C_{max}) of 2.7 μg/mL and an area under the curve (AUC) of 4.9 h·μg/mL at a 10 mg/kg P.O. dose, and a favorable oral bioavailability with a value of 35% (Fig. 5A, B). We then assessed the pharmacodynamic (PD) efficacy of Pro-BA in H3122 xenograft tumors in nude mice. Our findings reveal that oral administration of Pro-BA at a dose of 25 mg/kg significantly lowered EML4-ALK levels after 48 h of treatment (Fig. 5C).

Given the promising PK/PD data, Pro-BA was further evaluated for its antitumor efficacy in the H3122 xenograft tumor mouse model via oral dosing. H3122 cells were injected subcutaneously into the right flank of female nude mice. After the tumors grew to an average volume of around 54 mm^3, the mice bearing H3122 tumors were randomly

https://doi.org/10.1038/s41467-025-60107-7

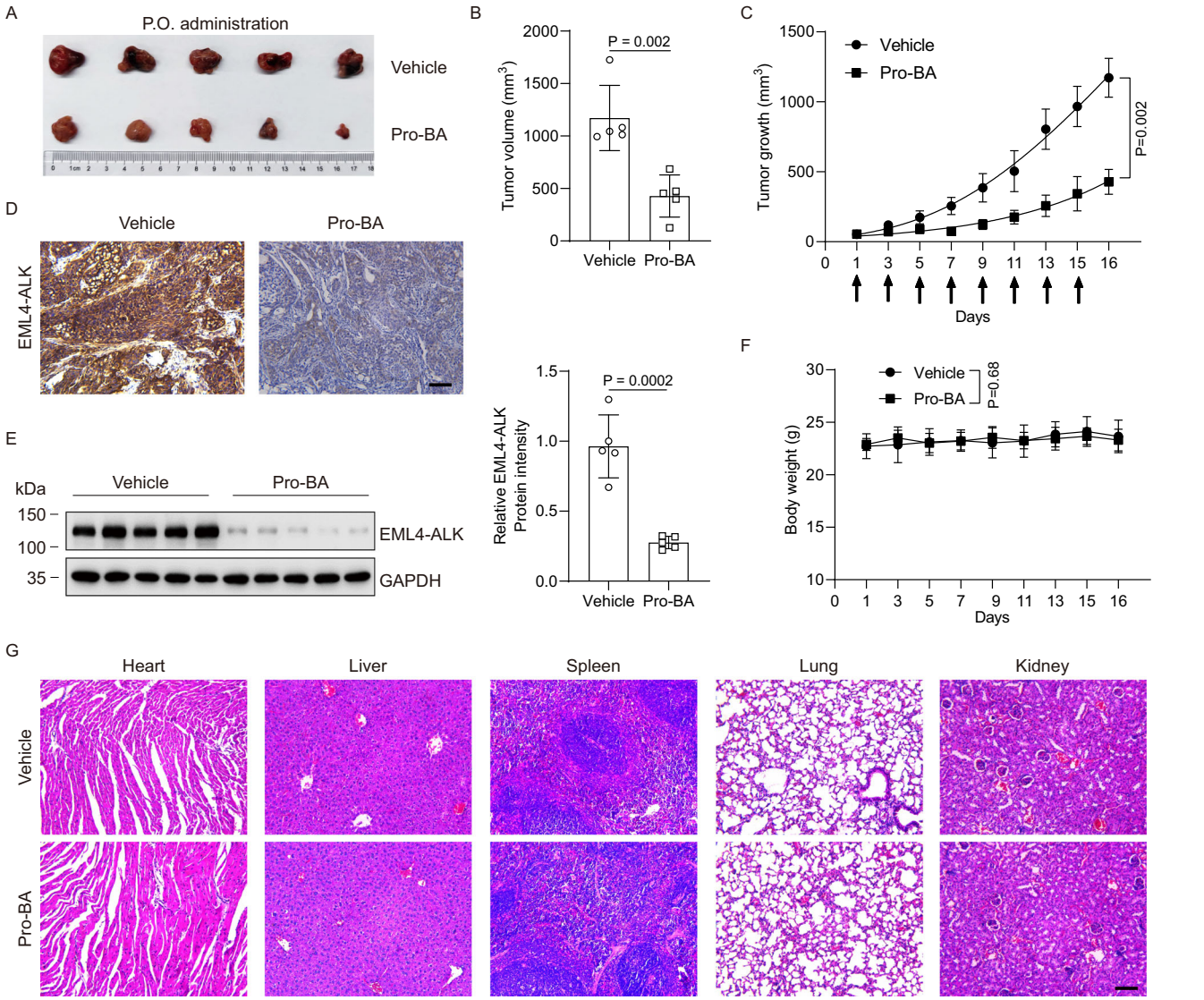

Fig. 6 | Pro-BA is an orally effective antitumor degrader. A H3122 cells were implanted into the right flank of 4-week-old female nude mice. The mice were treated with vehicle (ddH_2O) and Pro-BA (25 mg/kg in ddH_2O) through P.O. route every two days for a total of 8 administrations. The tumors were then surgically extracted and photographed. **B** The bar graph illustrates the mean ± SD of the primary tumor volumes of mice in (**A**). **C** The graph depicts the average tumor growth of mice in (**A**), delineated by black arrows for the treatment time points. Data is presented as the mean ± SEM ($n = 5$ mice per group), two-tailed Student's t-test. **D** Representative immunohistochemical staining of EML4-ALK in tumor sections of mice from (**A**), scale bar: 100 μm. **E** Immunoblot analysis of EML4-ALK protein levels was performed in tumor samples collected on day 16 following the initiation of oral administration (left panel). The bar graph provides a quantitative analysis of EML4-ALK protein levels based on the western blot images (right panel). **F** The graph illustrates the average body weight of mice administered via the oral route as described in (**C**). Data is shown as the mean ± SD ($n = 5$ mice per group), two-tailed Student's t-test. **G** Representative H&E staining of organs (heart, liver, spleen, lung, and kidney) from H3122 tumor-bearing mice administered orally with vehicle or Pro-BA, scale bar: 100 μm. For (**B**), (**E**) data are presented as the mean ± SD ($n = 5$ mice per group), two-tailed Student's t-test. Source data are provided as a Source Data file.

allocated into two groups and orally administered either vehicle or Pro-BA (25 mg/kg) every 2 days for eight treatments in total. The tumors were surgically resected and photographed the day after the last administration (Fig. 6A). We found that Pro-BA effectively shrank tumor volume and suppressed tumor growth (Fig. 6B, C). Immunohistochemistry and immunoblot analysis revealed that Pro-BA caused a notable reduction in EML4-ALK protein levels in tumors (Fig. 6D, E). No apparent body weight alterations were detected in mice treated with Pro-BA (Fig. 6F), and H&E staining showed intact morphology in the heart, liver, spleen, lung, and kidney in both the control and treatment groups (Fig. 6G), indicating that oral administration of Pro-BA exhibited no obvious toxicity and excellent tolerability in mice. Taken together, our data suggest that Pro-BA is a potent and orally bioavailable degrader.

The exploration of linker-free degraders for other targets

We wonder whether this linker-free degrader strategy can be extended to other target proteins. We applied this approach to the BCR-ABL fusion protein, a principal driver of chronic myeloid leukemia (CML). To facilitate the attachment of single amino acid-based degron to the BCR-ABL ligand, we designed a Dasatinib analog (DA), an analog of the BCR-ABL inhibitor Dasatinib, by removing the hydroxyethyl group from the piperazine ring of Dasatinib exposed on the protein's surface, based on the co-crystal structure of BCR-ABL and Dasatinib (Fig. 7A, B). Next, we separately appended Pro and Gly to DA, developing two linker-free BCR-ABL degraders: Pro-DA and Gly-DA (Fig. 7C). To evaluate the effective concentrations of these linker-free degraders on the degradation of BCR-ABL, the K562 cells were treated with Pro-DA and Gly-DA individually at various concentrations for 48 h. We found that

https://doi.org/10.1038/s41467-025-60107-7

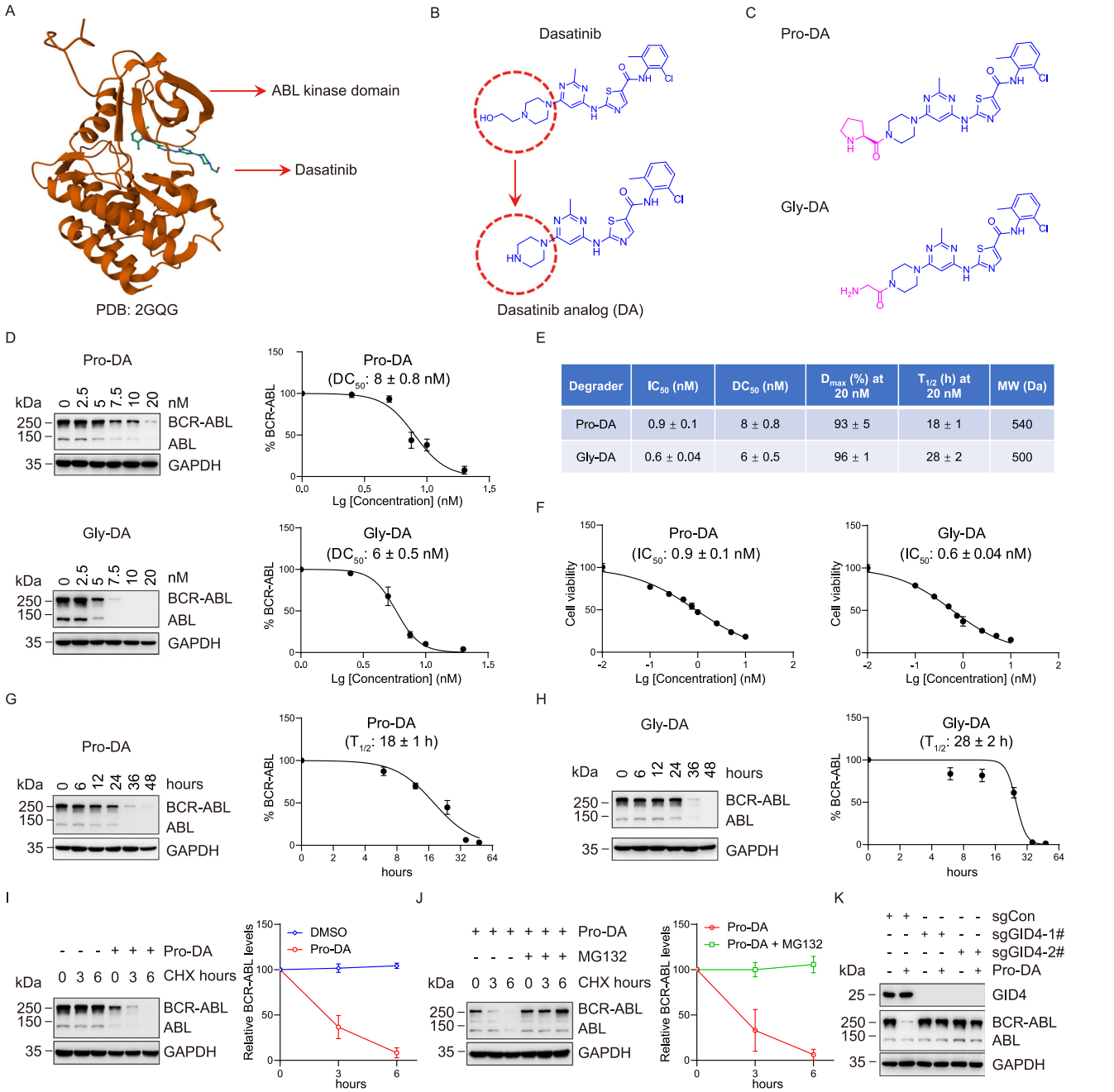

Degrader	IC_{50} (nM)	DC_{50} (nM)	D_{max} (%) at 20 nM	$T_{1/2}$ (h) at 20 nM	MW (Da)
Pro-DA	0.9 ± 0.1	8 ± 0.8	93 ± 5	18 ± 1	540
Gly-DA	0.6 ± 0.04	6 ± 0.5	96 ± 1	28 ± 2	500

Fig. 7 | Characterization of BCR-ABL-targeting linker-free degraders. A Crystal structure of ABL in complex with Dasatinib (PDB: 2GQG). **B** The structures of Dasatinib and Dasatinib analog (DA). **C** The structures of Pro-DA and Gly-DA. **D** K562 cells were separately treated with Pro-DA or Gly-DA at the indicated concentration for 48 h, followed by immunoblot analysis of BCR-ABL and GAPDH protein expression (left panel). The plots were utilized to determine the DC_{50} values by quantifying BCR-ABL protein levels (right panel). **E** Summary of DC_{50}, D_{max}, IC_{50}, $T_{1/2}$ values, and molecule weight (MW) for Pro-DA and Gly-DA. **F** K562 cell viability was assessed using CCK-8 assays following a 48-h treatment with varying concentrations of Pro-DA and Gly-DA. **G**, **H** Immunoblot analysis was performed on K562 cells treated with Pro-DA (**G**) and Gly-DA (**H**) at 20 nM for various time points (left panel). The curves were used to calculate the $T_{1/2}$ values of Pro-DA (**G**) and Gly-DA (**H**) by quantifying BCR-ABL protein levels (right panel). **I** K562 cells were exposed to 10 nM Pro-DA for 30 h, followed by incubation with CHX (100 μg/mL) at specified time points. BCR-ABL stability was assessed by immunoblotting (left panel), and the intensity of BCR-ABL protein bands was quantified (right panel). **J** K562 cells were treated with 20 nM Pro-DA for 30 h, then CHX (100 μg/mL) was added for the indicated times in the presence or absence of MG132. BCR-ABL stability was evaluated by immunoblotting (left panel), with band intensity quantified (right panel). **K** K562 cells with stable expression of sgCon, sgGID4-1#, or sgGID4-2# were incubated with DMSO or Pro-DA (20 nM) for 48 h, and the indicated protein levels were assessed by immunoblotting. For (**D**), (**F**), (**G**), (**H**), (**I**), (**J**), the data are shown as mean ± SD derived from three independent experiments. Source data are provided as a Source Data file.

both compounds were highly potent, achieving robust degradation of BCR-ABL at nanomolar concentrations. Pro-DA efficiently degraded BCR-ABL in K562 cells, with a DC_{50} value of 8 nM, and achieving a 93% reduction at 20 nM (Fig. 7D upper panel, 7E and Supplementary Fig. 5A). Gly-DA effectively reduced BCR-ABL in K562 cells, with a DC_{50} value of 6 nM, and attained a 96% reduction at 20 nM (Fig. 7D, lower panel, 7E and Supplementary Fig. 5B). Pro-DA and Gly-DA also exhibited excellent growth inhibition, with IC_{50} values of 0.9 nM and 0.6 nM, respectively (Fig. 7E, F). Moreover, Pro-DA started lowering BCR-ABL protein levels from the 6th hour, with a half-life of 18 h (Figs. 7E, G and

Supplementary Fig. 5C), while Gly-DA initiated the reduction around the 6th hour, with a half-life of 28 h (Figs. 7E, H and Supplementary Fig. 5D). These results indicate that Pro-DA promotes faster protein elimination.

We then monitored the degradation kinetics of BCR-ABL in the presence and absence of Pro-DA. Cycloheximide was applied to K562 cells to inhibit new protein production, and residual BCR-ABL protein amounts were assessed at different time points. BCR-ABL protein levels exhibited a rapid decline in cells exposed to Pro-DA, whereas they remained largely unchanged in cells treated with DMSO (Fig. 7I and Supplementary Fig. 5E). Furthermore, Pro-DA-induced turnover of BCR-ABL was blocked by the proteasome inhibitor MG132 (Fig. 7J and Supplementary Fig. 5F). The Pro-DA-mediated decrease of BCR-ABL protein levels was largely blunted in GID4 knockout K562 cells (Fig. 7K).

Subsequently, we evaluated the performance of the linker-free Gly-DA and the linker-bearing Gly-PEG1-DA (Supplementary Fig. 6A). To this end, K562 cells were exposed to Gly-DA and Gly-PEG1-DA at 5 nM and 7.5 nM. Results showed that Gly-PEG1-DA did not induce BCR-ABL degradation, unlike Gly-DA, which effectively degraded BCR-ABL at both concentrations (Supplementary Fig. 6B). We further treated K562 cells with varying concentrations of Gly-PEG1-DA and found that even at 20 nM, it had no effect on BCR-ABL protein levels (Supplementary Fig. 6C). The CCK-8 cell viability assay showed that Gly-PEG1-DA had an IC_{50} value of 21 nM, ~40 times less potent than Gly-DA (Supplementary Fig. 6D). Collectively, these observations suggest that Gly-DA is significantly more potent in comparison to Gly-PEG1-DA incorporating one unit of PEG linker.

To further investigate the activity of Gly-DA, we assessed its effect in another BCR-ABL fusion-positive CML cell line, KU812. The results showed that Gly-DA efficiently induced BCR-ABL turnover, with a DC_{50} of 1.2 nM (Supplementary Fig. 7A). BCR-ABL degradation was observed as early as 1 h, with a $T_{1/2}$ of about 5 h (Supplementary Fig. 7B). Unlike Gly-DA, the unmodified ABL inhibitor Dasatinib did not alter BCR-ABL levels at the same time points (Supplementary Fig. 7C). Additionally, the CCK8 assay revealed that Gly-DA began to inhibit cell proliferation at 3 h post-treatment (Supplementary Fig. 7D), whereas Dasatinib exhibited an inhibitory effect as early as 1 h post-treatment (Supplementary Fig. 7E). These data indicate that the degradation of BCR-ABL and the antiproliferation effects, induced by Gly-DA, take place on the same timescale. Flow cytometry analysis further revealed that Gly-DA increased the proportion of both early and late apoptotic cells at 3 h, with no significant changes detected before 1 h (Supplementary Fig. 7F, G). Overall, the data indicate that Gly-DA-mediated BCR-ABL degradation and cell death occur within a closely aligned timeframe, with degradation initiating marginally earlier than the onset of apoptosis. The brief time gap between these events suggests that their progression is largely synchronized.

Discussion

Despite recent advancements in TPD technology, it still faces several challenges, such as the large molecular size of modular PROTACs and the randomness in the development of MGs, which limit their broader application[3,5]. In this study, we demonstrate the efficacy of linker-free PROTACs by directly coupling single amino acids, the simplest degradation signal, to several ligands of the target protein without the need for a bridging linker. Our strategy not only reduces the molecular weight of PROTACs to levels similar to MGs but also offers a simplified and modular design.

Although the functionality of PROTACs obviously comes from the ligands on the two ends that bring E3 ligases and target proteins together, the variations in linker length and chemical composition clearly also impact the physicochemical properties and efficiency of PROTACs[20,21,34]. Nevertheless, a universal strategy for the linker design in PROTACs has yet to be established. PROTACs featuring longer linkers tend to be more effective at facilitating the degradation of target proteins. For example, PROTACs with longer carbon chains exhibit stronger degradation activity against ENL[35]. Xue et al. developed the ENL-targeting PROTACs with carbon (C) linkers of 2C to 11C and observed that PROTACs with 2C to 6C were ineffective, whereas those with carbon chain lengths greater than 6C were generally effective[35]. On the other hand, Wurz and colleagues found that a longer linker in SMARC1 and BRD4 PROTACs decreased the synergy of the POI-PROTAC-E3 ternary complex, leading to a decrease in target protein degradation efficiency[33]. Interestingly, Cyrus et al. designed PROTACs targeting ERα with varying alkyl lengths and found that a 16-atom linker length achieved the best performance, with both shorter and longer linkers being less effective[21]. The critical role of a linker is not surprising since the successful PROTAC does not just bring the substrate and E3 ligase together but also ensures the spatial positioning of the PROTAC-mediated ternary complex is conducive to substrate ubiquitylation. Thus, an appropriate linker can play a key role in promoting a productive engagement between the substrate and E3 ligase.

For the reasons described above, most of the PROTAC studies start with tinkering with the identity and length of the linkers. To our knowledge, in nearly all cases so far, the linkers are essential parts of the PROTACs despite serving as an accessory facilitators. Some studies examined the linker-free PROTACs, which appeared to be inefficient[36–38]. For example, Li and colleagues created a compound 3 without a linker by merging the MDM2 ligand MI-1061 with the CRBN ligand lenalidomide directly, but it was unable to degrade MDM2[36]. In contrast, similar compounds bearing flexible linkers of varying lengths successfully induced MDM2 degradation[36]. As our work demonstrates that a linker is not an essential requirement for effective PROTACs, contrary to the prevailing view, this study shifts the focus of the field toward optimizing various factors involved in a productive target-PROTAC-E3 complex, with or without linkers, including binding kinetics, ubiquitylation efficiency, and spatial and temporal regulation. Unlike traditional PROTACs, we have created small and effective linker-free AATacs (e.g., Pro-BA, Gly-BA, Pro-DA), narrowing the gap between PROTACs and MGs. It is tempting to speculate that PROTACs using other types of degrons (e.g., CRBN- or VHL-based) may work well without the linkers as well in some cases. As difficult as it is to get the right linker for a PROTAC design, it is perhaps challenging to find the right combination of the target and E3 ligase without the need for a linker for a non-AATac.

The larger size of the PROTACs has spurred efforts to find small and designable degraders. For example, a series of BRD4-targeting degraders have been engineered to introduce a gain-of-function neointeraction between BRD4 and an E3 ligase DCAF16 or CTLH by adding a small chemical moiety to JQ1[25–29]. Similarly, the Nomura group identified covalent handles for the E3 ligases DCAF16 and RNF126, which can be directly fused with various protein-targeting ligands, thereby inducing the degradation of the respective target proteins without requiring a linker[22–24]. They have described such covalent degraders as “monovalent degraders” or “molecular glue degraders”, yet they also note that these molecules could be classified as “bivalent degraders” or “mini-PROTACs” due to their independent binding to both the target proteins and E3 ligase (DCAF16 or RNF126). These findings support the notion that an intermediate linker is not always a mandatory component for the functionality of PROTACs and imply that, with the ongoing advancements in molecular glue and PROTAC strategies, the distinction between these two classes of degraders will likely become increasingly blurred. However, different from the approaches involving the screening of covalent handles and corresponding E3 ligase identification via chemoproteomics and activity-based protein profiling (ABPP), our strategy leverages the existing cellular N-degron degradation

pathway that is conserved across species from bacteria to animals, offering a simpler and more straightforward method for TPD.

While considerable work has been devoted to improving the oral bioavailability of PROTACs, a standardized method for optimization remains unavailable[39,40]. The large molecular weight of PROTACs significantly hinders their oral bioavailability by affecting absorption, solubility, metabolism, and membrane permeability[41,42]. The linker-free covalent degraders[22,23], while reducing PROTAC molecular size, still lack comprehensive pharmacokinetic and pharmacodynamic evaluations. In our study, the linker-free Pro-BA is water-soluble and shows a favorable pharmacokinetic profile and good oral bioavailability in mice. Pro-BA effectively suppressed tumor growth when administered orally, with no significant toxicity observed. We have demonstrated that the linker-free AATac (i.e., Pro-BA) is effective in vivo, showcasing its potential for oral administration and tumor inhibition without the need for traditional linkers.

The majority of the PROTACs developed thus far employ limited degrons and E3 ligases (e.g., CRBN, VHL). We have explored the adaptation of N-degrons in TPD[8–10,43]. Nineteen amino acids, other than Met, can directly serve as a potent degron to recruit various E3 ligases to mediate substrate degradation via the N-end rule pathway[11–17]. These amino acid-based degrons offer unique advantages including: (1) their small size, ranging from 75 to 204 Da, whereas other degrons are often over 250 Da[44]; (2) interchangeability with different properties (e.g., charge, hydrophobicity); (3) the ability to attract different E3s with distinct expression patterns. Our demonstration of the efficiency of the linker-free AATacs against multiple targets (e.g., EML4-ALK and BCR-ABL) makes this approach an attractive option in TPD. In summary, the linker-free AATacs developed in this study offer a streamlined and modular design that substantially shrinks PROTACs to a size akin to small-molecule drugs with a favorable oral bioavailability. Future optimization will be necessary to further enhance their efficacy, target specificity, and adaptability, establishing the linker-free AATacs as a broadly applicable scaffold for degrader design.

Methods

Reagents

Antibodies used include anti-ALK (3633, 1:2000), anti-c-Abl (2862, 1:1000), anti-myc-tag (2040, 1:2000 dilution), anti-HA-tag (2999, 1:2000) obtained from Cell Signaling Technology; anti-GAPDH (HRP-60004, 1:6000), anti-α-Tubulin (HRP-66031, 1:6000) acquired from Proteintech; anti-GID4 (NBP1-53184, 1:500) obtained from Novus. And anti-Flag (A8592) and anti-FLAG® M2 Magnetic Beads (M8823) were purchased from Sigma. MG132, cycloheximide, and Brigatinib were obtained from MedChemExpress. Dasatinib was purchased from Energy Chemical.

Compounds

The synthesis procedures for all compounds are provided in the supplementary data.

Cell culture

H3122 was purchased from Meisen Chinese Tissue Culture Collection (MeisenCTCC, China). K562 and HEK293T cell lines were purchased from the American Type Culture Collection (ATCC, USA). KU812 was purchased from Guangzhou Xinyuan Biotechnology Co., Ltd (Biospecies, China). BaF3-EML4-ALK was generously gifted by Professor Xianming Deng (School of Life Sciences, Xiamen University). H3122, K562, KU812, and BaF3-EML4-ALK were maintained in RPMI1640 (Thermo Scientific™) plus 10% fetal bovine serum (FBS) (Transgen) and penicillin, streptomycin (Beyotime). HEK293T was cultured in DMEM (Thermo Scientific™) plus 10% FBS and penicillin, streptomycin. Mycoplasma testing of cell culture was performed routinely using a MycoBlue Mycoplasma Detector Kit (Vazyme, China).

Constructs

Full-length GID4 was inserted into the EcoRI and BamHI sites of the pLVX-IRES-neo vector, fused to an N-terminal 3× HA tag. GID4 was also cloned into the EcoRI site of the pHTN vector, with an N-terminal HaloTag fusion. The ALK fragment (residues 1094-1400) was cloned into the EcoRI site of the pNLF1-N vector, fused to the N-terminal NanoLuc. The plasmid pCMV-myc-Ub was purchased from MiaoLing Biology (Cat#: P25115). The pCDH-CMV-Flag-EML4-ALK V1-EF1-puro lentiviral plasmid was generously gifted by Professor Hongbin Ji (Center for Excellence in Molecular Cell Science, Chinese Academy of Sciences). All sgRNA sequences were inserted into the BsmBI site of the lentiCRISPR v2 vector (#52961, Addgene), following the Addgene protocol.

Immunoblot analysis

Cells were harvested and lysed in RIPA buffer (50 mM Tris-HCl, pH 8.0, 1% NP-40, 150 mM NaCl, 0.1% SDS, 0.5% sodium deoxycholate, and 1× complete protease inhibitor cocktail) on ice for 30 min. The lysates were then centrifuged at 21,130 × *g* for 10 min at 4 °C to obtain the supernatant. Protein concentrations were determined using the BCA protein assay kit (Beyotime). Equal amounts of proteins from each sample were mixed with loading buffer, denatured by boiling, and subjected to SDS-PAGE. The proteins were then transferred to PVDF membranes, which were blocked with 5% non-fat milk for 1 h at room temperature. The membranes were incubated with primary antibodies overnight at 4 °C, followed by incubation with HRP-conjugated secondary antibodies for 1 h at room temperature. Protein detection was performed using ECL reagent (Millipore) and visualized with a Tanon-5200 Automatic Chemiluminescence Imaging System (Tanon, China).

The co-immunoprecipitation assay

HEK293T cells cotransfected with HA-GID4 and Flag-EML4-ALK were treated with DMSO, Brigatinib, Pro-BA, or Pro-PEG3-BA for 24 h. Then the cell lysates were prepared by incubating the cells in lysis buffer (50 mM Tris–HCl, pH 8.0, 0.2% NP-40, 150 mM NaCl, 2 mM EDTA, and 1× complete protease inhibitor cocktail) for 20 min at 4 °C, followed by centrifugation at 14,000 × g for 15 min at 4 °C. A 5% aliquot of the whole-cell lysates (WCL) was taken as input, while the remaining lysate was incubated with 10 µL of anti-FLAG® M2 Magnetic Beads for 4 h at 4 °C. Beads were then washed five times using the cold lysis buffer. The immunoprecipitates were boiled with 2× SDS-PAGE loading buffer, separated on SDS-PAGE gels, followed by immunoblotting with various antibodies indicated.

The ubiquitylation assay

HEK293T cells co-expressing HA-GID4, Flag-EML4-ALK, and myc-Ub were subjected to DMSO, Brigatinib, Pro-BA, or Pro-PEG3-BA treatments for 24 h, followed by a 4-h MG132 exposure. Ubiquitination of EML4-ALK was then detected using denatured immunoprecipitation. Cells were lysed in SDS-denaturing buffer (50 mM Tris–HCl [pH 7.4], 150 mM NaCl, 1% NP-40, 1% SDS, and 0.5% sodium deoxycholate) and boiled for 10 min. Cell lysates were then diluted 10-fold in native lysis buffer (50 mM Tris–HCl [pH 7.4], 150 mM NaCl, 1% NP-40, and 0.5% sodium deoxycholate). After centrifugation at 21,130 × g for 10 min, the supernatants were immunoprecipitated using anti-FLAG® M2 Magnetic Beads and incubated for 4 h at 4 °C. Beads were then washed five times using the native lysis buffer. The immunoprecipitates were boiled with 2× SDS-PAGE loading buffer, separated on SDS-PAGE gels, followed by immunoblotting with various antibodies indicated.

Lentiviral production and infection

A lentiviral vector carrying the sgRNA was co-transfected into HEK293T cells along with a packaging vector (psPAX2) and an envelope vector (pMD2.G) using polyethylenimine. Virus-containing

supernatants were collected at 48 h post-transfection, and filtered through 0.45 μm filters to remove cell debris. The viruses were used to infect target cells grown in medium supplemented with 8 μg/mL polybrene. Infected cells were then obtained in the presence of 1 μg/mL puromycin. The sgRNA targeting sequences used were: sgGID4-1#, GCTCTACAGCGGCTCCAAGT; sgGID4-2#, GGGGAACTCGTACGACGTAG.

Cell viability assay

Cells were cultured in 96-well plates with 100 μL of medium at a density of 5×10^3 per well. Following a 48-h treatment with the indicated compounds at different concentrations, CCK-8 solution was added and incubated for 2 h at 37 °C. The viability of cells was evaluated by measuring absorbance at 450 nm, as per the manufacturer's guidelines (Transgen).

Cell cycle and apoptosis assays

H3122 cells (1.5×10^5 cells per well) were seeded in 6-well plates. Next day, cells were exposed to the Pro-BA, Pro-PEG1-BA or Pro-PEG3-BA at 500 nM for 24 h. For cell cycle assays, the media were removed, and cells were washed three times with PBS. Then cells were harvested and fixed in ice-cold 70% ethanol for 2 h at 4 °C. The fixed cells were washed again with cold PBS and then stained with PI (Beyotime, Cell Cycle and Apoptosis Analysis Kit, C1052) for 30 min at 37 °C . Subsequently, the cell cycle was analyzed by flow cytometry with BD FACSCanto SORP. For cell apoptosis assays, both cells and media were gathered and washed once with PBS. The cells were then resuspended in Binding Buffer and stained with FITC and PI using the Annexin V-FITC Apoptosis Detection Kit (Beyotime, C1062) for 15 min in the dark at room temperature. Cell apoptosis was subsequently assessed using a BD FACSCanto SORP.

Protein expression and purification

For ALK in mammalian cell expression, the N-terminal Strep-Strep-Flag tag human ALK kinase domain (residues 1094–1400) was cloned into the pCAG vector using KpnI and XhoI restriction sites. The Expi293F cells were grown in Union-293 medium (UP1000, Union-Biotech Co., Ltd) and transfected with 1 mg DNA and 3 ml PEI (78PEI40000, Biohub) per 1 liter of cells at a density of 2×10^6 cells/mL. Cells were harvested after 60 h and washed with 1× cold PBS. Then the cell pellets were resuspended in lysis buffer (20 mM HEPES pH 7.4, 200 mM NaCl, 2 mM $MgCl_2$, 0.5 mM TCEP, 1% (v/v) Triton-X 100) with protease inhibitors (1 mM PMSF, 0.15 μM aprotinin, 10 μM leupeptin, 1 μM pepstatin) for 30 min. After centrifugation at 16,000 × *g* for 50 min at 4 °C, the cell supernatant was incubated with Strep-Tactin Sepharose beads (2-1201-010, IBA) at 4 °C for 2 h. The beads were washed with wash buffer (20 mM HEPES pH 7.4, 200 mM NaCl, 2 mM $MgCl_2$, 0.5 mM TCEP, 2 mM ATP). Bound proteins were eluted with wash buffer containing 10 mM Desthiobiotin (2-1000-005, IBA). The protein elution was further purified by Superdex200 Increase 10/300 GL column (Cytiva) equilibrated in gel filtration buffer (20 mM HEPES pH 7.4, 200 mM NaCl, 2 mM $MgCl_2$, 0.5 mM TCEP). The protein sample was flash frozen in liquid nitrogen and stored at −80 °C until use.

Isothermal titration calorimetry (ITC) analysis

ITC assays were conducted at 25 °C using a MicroCal PEAQ-ITC instrument (Malvern Panalytical). Purified ALK protein fragment (residues 1094-1400), Pro-BA or Pro-PEG3-BA were dissolved in an identical buffer (20 mM HEPES, 200 mM NaCl, 2 mM $MgCl_2$, 0.5 mM TCEP). Pro-BA (100 μM in syringe) or Pro-PEG3-BA (100 μM in syringe) was titrated separately into the protein solution (5 μM in cell) with 19 injections of 2 μL each, except for the initial injection of 0.4 μL, with an interval of 150 s between injections and a reference power setting of 10 μcal/s. Analysis of the ITC data was carried out with MicroCal PEAQ-ITC Analysis Software.

Quantitative proteomics

Cell culture and lysis: H3122 cells were treated with DMSO or 500 nM Pro-BA for 12 h. The cells were lysed in urea buffer containing concentration of 8 M urea and EDTA-free protease inhibitor (Sigma-Aldrich, USA) by scraping and sonication. Then, the cells were cleaned up by centrifugation at 21,000 × *g* for 20 min at 4 °C, and the supernatants were collected. The BCA assay (Thermo Fisher Scientific) was used for quantifying protein concentration.

Sample Preparation and MS analysis: The samples were prepared by SISPROT as previously described. Data were acquired by Orbitrap Exploris 480 mass spectrometer (Thermo Fisher Scientific) with an UltiMate 3000 HPLC system (Thermo Fisher Scientific) and a 20 cm × 100 μm i.d. analytical column in-house packed with C18 beads (1.9 μm/120 Å, Dr. Maisch GmbH). The flow rate was set as 3 μL/min for sample loading and 300 nL/min for separation. Peptides were separated with a binary buffer system of 0.1% (v/v) formic acid (buffer A) and ACN/0.1% (v/v) formic acid (buffer B). A 120 min total LC gradient was programmed: 2–6% buffer B in 1 min, 6–22% buffer B in 106 min, 22–36% buffer B in 8 min, 36–80% buffer B in 2 min, and finally equilibration with 98% buffer B for 3 min. MS parameters were as follows: Full MS scans over the *m/z* range of 350–1250 were performed at a resolution of 60,000. The Orbitrap Exploris 480 was operated in a data-dependent mode. Full scan and top 40 MS/MS scans were acquired per cycle with an MS1 scan resolution of 60,000 and an MS/MS scan resolution of 15,000. HCD fragmentation was set with a normalized collision energy (NCE) of 28.

Peptide Identification: Raw MS data were processed using MaxQuant software (version 2.4.7.0) against the human UniProt FASTA database (downloaded on 23 July 2023, with 20,241 entries). The label-free quantification (LFQ) was enabled, and default settings were set. Carbamidomethyl was added as static modification. Met-loss (M), Met-loss + Acetyl (M), and Acetyl (Protein N-term) were added as variable modifications. The false discovery rate (FDR) was set to 0.01.

Data processing: Before conducting the analysis, a stringent criterion was employed to ensure the reliability of the mass spectrometry (MS) results. Specifically, only proteins with at least two peptide-spectrum matches (PSMs) were retained, and contaminant proteins were filtered out. For normalization to the overall proteomic data, it was assumed that samples treated under the same experimental procedure, although some proteins may exhibit variations upon drug treatment, would maintain a consistent overall proteomic level. For each dataset in both the control and treatment groups, the median values were calculated separately. Subsequently, to achieve uniform median values within the same group, each dataset was normalized by dividing it by a constant factor as necessary.

To identify differentially degraded proteins between the control and treatment groups, we conducted a significance analysis using the LIMMA package in R (R version 4.3.0). This powerful statistical tool enabled us to robustly assess the differences in proteomic levels. We calculated both p-values and logFC (logarithmic fold change) values for each protein. By setting a threshold of $p < 0.05$, we were able to rigorously filter out proteins that exhibited significant changes in degradation.

NanoBRET cellular ternary complex formation assay

HEK293T cells (8×10^5) were co-transfected with 2 μg of HaloTag-GID4 plasmids (pHTN-GID4) and 0.2 μg of NanoLuc-ALK vectors (pNLF1-N-ALK). The following day, 2×10^5 of the transfected cells were reseeded into 96-well plates and incubated for 24 h with or without 100 nM HaloTag® NanoBRET® 618 Ligand (Promega). The cells were then incubated with different concentrations of Pro-BA or Pro-PEG3-BA for 6 h. BRET signals were measured 10 min following the addition of NanoBRET® Nano-Glo® Substrate. To calculate NanoBRET ratios, background signals from cells without HaloTag® NanoBRET® 618 Ligand were subtracted from those with the ligand. The resulting

values were expressed in milliBRET units (mBU), representing the ratio of acceptor signal (618 nm) to donor signal (460 nm), multiplied by 1000. The fold increase in BRET signal was calculated by dividing the mBRET ratios from Brigatinib, Pro-BA, or Pro-PEG3-BA-treated cells by the average mBRET ratios from DMSO-treated cells, to assess the potential for intracellular ternary complex formation.

Solubility determination of Pro-BA

Pipette 100 µL of water into a centrifuge tube, add an excess amount of the compound Pro-BA, and shake at constant temperature for 30 min. Centrifuge and collect the supernatant. Determine the corresponding concentration of the saturated solution based on its peak area on the calibration curve of Pro-BA. The concentration of Pro-BA was measured to be 1.8 M. The concentration of Pro-PEG3-BA was measured to be 0.86 M according to the same procedure.

Pharmacokinetic (PK) and pharmacodynamic (PD) studies of Pro-BA

For the PK study, Pro-BA was dissolved in ddH_2O and delivered either via intravenous (I.V.) injection at 2 mg/kg ($n = 3$ mice) or orally (P.O.) at 10 mg/kg ($n = 3$ mice). Blood samples were drawn from the retro-orbital venous plexus of mice into EDTA-K2 tubes at intervals of 0.083, 0.25, 0.5, 1, 3, 6, 8, 10, and 12 h following the drug treatment. The collected blood samples were then centrifuged at 845 × *g* for 10 min at 4 °C to yield supernatant plasma samples. The Pro-BA plasma levels were quantified by HPLC, and the PK parameters were calculated through the noncompartmental model using Phoenix WinNonlin 8.1.

For the PD study, H3122 tumor-xenografted nude mice were treated with either vehicle (ddH_2O) or Pro-BA at 10 mg/kg in ddH_2O via oral administration when the tumor volume reached around 100 mm^3. After 48 h, the mice were sacrificed, and the tumor tissues were collected for immunoblot analysis.

The BALB/c mice and nude mice were obtained from GemPharmatech Co., Ltd, (China). All animal experiments were conducted with approval from the Animal Care Committee of Southern University of Science and Technology.

Mouse xenograft models

Comparison of in vivo antitumor effects of Pro-BA and Pro-PEG3-BA. H3122 cells (1×10^7 cells/200 µL) were subcutaneously implanted into the right flank of 4-week-old female nude mice. Upon tumors reaching a palpable size of around 45 mm^3, the mice were randomly allocated into four groups: vehicle, Brigatinib, Pro-PEG3-BA, and Pro-BA, with five mice per group. The treatments, including vehicle, Brigatinib, Pro-PEG3-BA, and Pro-BA (10 mg/kg, prepared in a solution of 90% corn oil +10% DMSO), were administered via I.P. injection every other day for a total of eight doses. The growth of tumors in mice was measured using a Vernier caliper. The tumor volume was calculated using the formula: volume = 0.5 × (length) × $(width)^2$. Mice harboring tumors were sacrificed the day after the final treatment, and then the tumors were excised and imaged.

Evaluation of the antitumor effect of orally administered Pro-BA. H3122 cells (1×10^7 cells/200 µL) were subcutaneously injected into the right flank of 4-week-old female nude mice. The mice were divided randomly into two groups: vehicle and Pro-BA (five mice per group), once the tumors achieved an average size of about 54 mm^3. The treatment was applied orally every two days, with either the vehicle (ddH_2O) or Pro-BA at 25 mg/kg dissolved in ddH_2O, for a cumulative total of 8 doses. The growth of tumors in mice was recorded with a Vernier caliper. The tumor volume was determined with the formula: volume = 0.5 × (length) × $(width)^2$. Mice carrying tumors were sacrificed following the final treatment, and then the tumors were harvested and photographed. The permitted maximum tumor burden of 2000 mm^3 was not exceeded during the course of the experiments.

The nude mice were purchased from GemPharmatech Co., Ltd, (China) and maintained in a specific pathogen-free animal facility in a condition-controlled room (23 ± 1 °C, 50 ± 10% humidity) with a 12 h light/dark cycle. All animal studies were approved by the Animal Care Committee at Southern University of Science and Technology.

Immunohistochemical (IHC) staining

IHC analysis was performed to evaluate EML4-ALK expression in H3122 xenograft tumor sections. Briefly, the tumor tissue sections were deparaffinized and rehydrated, then subjected to antigen retrieval through heating in a Tris–EDTA buffer (pH 9.0) at 95 °C for 20 min. Endogenous peroxidase activity was quenched using an endogenous peroxidase inhibitor (ZSGB-BIO) for 10 min. The sections were blocked with goat serum for 30 min, followed by an overnight incubation at 4 °C with anti-ALK antibody (CST, 3633, 1:100 dilution). Afterward, secondary antibodies (Proteintech) were applied for 1 h, and the sections were developed with 3,3′-diaminobenzidine (DAB). The nuclei were counterstained with Hematoxylin.

H&E staining

The tissue sections from various organs (heart, liver, spleen, lung, and kidney) of H3122 tumor-bearing mice, which were treated with orally administered vehicle or Pro-BA, were deparaffinized and stained using the Hematoxylin and Eosin Staining Kit (Beyotime, C0105S) according to the manufacturer's instructions.

Statistical analysis

The data represent the mean ± SD or SEM values of samples obtained from three independent experiments. We performed comparisons between groups using a two-tailed Student's *t*-test or a one-way ANOVA, as specified in the figure legends. Statistical analysis of quantitative proteomics data was performed using the LIMMA package. In the statistical analysis, $p < 0.05$ is deemed as statistically significant.

Reporting summary

Further information on research design is available in the Nature Portfolio Reporting Summary linked to this article.

Data availability

All the raw mass spectrometry data have been deposited to the ProteomeXchange Consortium via the iProX partner repository[45,46] with the dataset identifier PXD062245. Source data are provided with this paper.

References

1. He, M. et al. PROTACs: great opportunities for academia and industry (an update from 2020 to 2021). *Signal. Transduct. Target. Ther.* **7**, 1–64 (2022).
2. Sathe, G. & Sapkota, G. P. Proteomic approaches advancing targeted protein degradation. *Trends Pharmacol. Sci.* **44**, 786–801 (2023).
3. Békés, M., Langley, D. R. & Crews, C. M. PROTAC targeted protein degraders: the past is prologue. *Nat. Rev. Drug Discov.* **21**, 181–200 (2022).
4. Sasso, J. M. et al. Molecular glues: the adhesive connecting targeted protein degradation to the clinic. *Biochemistry* **62**, 601–623 (2022).
5. Dewey, J. A. et al. Molecular glue discovery: current and future approaches. *J. Med. Chem.* **66**, 9278–9296 (2023).
6. Domostegui, A., Nieto-Barrado, L., Perez-Lopez, C. & Mayor-Ruiz, C. Chasing molecular glue degraders: screening approaches. *Chem. Soc. Rev.* **51**, 5498–5517 (2022).
7. Cao, C., He, M., Wang, L., He, Y., Rao, Y. Chemistries of bifunctional PROTAC degraders. *Chem. Soci. Rev.* **51**, 7066–7114 (2022).

8. Shanmugasundaram, K. et al. A modular PROTAC design for target destruction using a degradation signal based on a single amino acid. *J. Biol. Chem.* **294**, 15172–15175 (2019).
9. Zhang, J. et al. Single amino acid–based PROTACs trigger degradation of the oncogenic kinase BCR–ABL in chronic myeloid leukemia (CML). *J. Biol. Chem.* **299**, 104994 (2023).
10. Zhang, J. et al. Distinct amino acid-based PROTACs target oncogenic kinases for degradation in non-small cell lung cancer (NSCLC). *J. Med. Chem.* **67**, 13666–13680 (2024).
11. Varshavsky, A. N-degron and C-degron pathways of protein degradation. *Proc. Natl Acad. Sci. USA* **116**, 358–366 (2019).
12. Bachmair, A., Finley, D. & Varshavsky, A. In vivo half-life of a protein is a function of its amino-terminal residue. *Science* **234**, 179–186 (1986).
13. Chen, S.-J., Wu, X., Wadas, B., Oh, J.-H. & Varshavsky, A. An N-end rule pathway that recognizes proline and destroys gluconeogenic enzymes. *Science* **355**, eaal3655 (2017).
14. Timms, R. T. et al. A glycine-specific N-degron pathway mediates the quality control of protein N-myristoylation. *Science* **365**, eaaw4912 (2019).
15. Yi, S. A., Sepic, S., Schulman, B. A., Ordureau, A., An, H. mTORC1-CTLH E3 ligase regulates the degradation of HMG-CoA synthase 1 through the Pro/N-degron pathway. *Mol. Cell* (2024).
16. Dong, C. et al. Recognition of nonproline N-terminal residues by the Pro/N-degron pathway. *Proc. Natl. Acad. Sci. USA* **117**, 14158–14167 (2020).
17. Li, Y. et al. CRL2ZER1/ZYG11B recognizes small N-terminal residues for degradation. *Nat. Commun.* **13**, 7636 (2022).
18. Sakamoto, K. M. et al. Protacs: chimeric molecules that target proteins to the Skp1–Cullin–F box complex for ubiquitination and degradation. *Proc. Natl. Acad. Sci. USA* **98**, 8554–8559 (2001).
19. Sakamoto, K. M. et al. Development of Protacs to target cancer-promoting proteins for ubiquitination and degradation. *Mol. Cell. Proteom.* **2**, 1350–1358 (2003).
20. Troup, R. I., Fallan, C. & Baud, M. G. Current strategies for the design of PROTAC linkers: a critical review. *Explor. Target. Anti Tumor Ther.* **1**, 273 (2020).
21. Cyrus, K. et al. Impact of linker length on the activity of PROTACs. *Mol. Biosyst.* **7**, 359–364 (2011).
22. Toriki, E. S. et al. Rational chemical design of molecular glue degraders. *ACS Cent. Sci.* **9**, 915–926 (2023).
23. Lim, M. et al. DCAF16-based covalent handle for the rational design of monovalent degraders. *ACS Central Sci.* **7**, 1318–1331 (2024).
24. Shishikura, K. & Matthews, M. L. Chemoproteomic covalent ligand discovery as the PROTAC-gonist: the future of targeted degradation medicines. *ACS Cent. Sci.* **10**, 1314 (2024).
25. Hassan, M. M. et al. Exploration of the tunability of BRD4 degradation by DCAF16 trans-labelling covalent glues. *Eur. J. Med. Chem.* **279**, 116904 (2024).
26. Li, Y.-D. et al. Template-assisted covalent modification underlies activity of covalent molecular glues. *Nat. Chem. Biol.* **20**, 1–10 (2024).
27. Shergalis, A. G. et al. CRISPR screen reveals BRD2/4 molecular glue-like degrader via recruitment of DCAF16. *ACS Chem. Biol.* **18**, 331–339 (2023).
28. Zhuang, Z. et al. Charged molecular glue discovery enabled by targeted degron display. *bioRxiv*. https://doi.org/10.1101/2024.09.24.614843 (2024).
29. Blake, R. et al. Preparation of tert-Butyl (S)-2-(4-(Phenyl)-6H-thieno [3, 2-f][1, 2, 4] triazolo [4, 3-a][1, 4]-diazepin-6-yl) acetate derivatives and related compounds as bromodomain BRD4 inhibitors for the treatment of cancer. *WIPO* https://patentscope.wipo.int/search/en/detail.jsf?docId=WO2020055976 (2020).
30. Bokhari, A. et al. Novel human-derived EML4-ALK fusion cell lines identify ribonucleotide reductase RRM2 as a target of activated ALK in NSCLC. *Lung Cancer* **171**, 103–114 (2022).
31. Crew, A. P. et al. Identification and characterization of Von Hippel-Lindau-recruiting proteolysis targeting chimeras (PROTACs) of TANK-binding kinase 1. *J. Med.Chem.* **61**, 583–598 (2018).
32. Imaide, S. et al. Trivalent PROTACs enhance protein degradation via combined avidity and cooperativity. *Nat. Chem. Biol.* **17**, 1157–1167 (2021).
33. Wurz, R. P. et al. Affinity and cooperativity modulate ternary complex formation to drive targeted protein degradation. *Nat. Commun.* **14**, 4177 (2023).
34. Bemis, T. A., La Clair, J. J. & Burkart, M. D. Unraveling the role of linker design in proteolysis targeting chimeras: miniperspective. *J. Med. Chem.* **64**, 8042–8052 (2021).
35. Xue, Z. et al. A potent and selective ENL degrader suppresses oncogenic gene expression and leukemia progression. *Sci. Adv.* **10**, eado1432 (2024).
36. Li, Y. et al. Discovery of MD-224 as a First-in-class, highly potent and efficacious PROTAC MDM2 degrader capable of achieving complete and durable tumor regression. *J. Med. Chem.* **62**, 448 (2019).
37. Meyers, M., Cismoski, S., Panidapu, A., Chie-Leon, B. & Nomura, D. K. Targeted protein degradation through recruitment of the CUL4 complex adaptor protein DDB1. *ACS Chem. Biol.* **19**, 58–68 (2024).
38. Hong, S. H. et al. Exploiting the cullin E3 ligase adaptor protein SKP1 for targeted protein degradation. *ACS Chem. Biol.* **19**, 442–450 (2024).
39. Poongavanam, V., Kihlberg, J. *PROTAC Cell Permeability and Oral Bioavailability: A Journey Into Uncharted Territory* (Taylor & Francis, 2022).
40. Zeng, S. et al. Current advances and development strategies of orally bioavailable PROTACs. *Eur. J. Med. Chem.* **261**, 115793 (2023).
41. Saraswat, A. L., Vartak, R., Hegazy, R., Patel, A. & Patel, K. Drug delivery challenges and formulation aspects of proteolysis targeting chimera (PROTACs). *Drug Discov. Today* **28**, 103387 (2023).
42. Guedeney, N., Cornu, M., Schwalen, F., Kieffer, C. & Voisin-Chiret, A. S. PROTAC technology: a new drug design for chemical biology with many challenges in drug discovery. *Drug Discov. Today* **28**, 103395 (2023).
43. Liu, Y., Wang, Z., Cang, Y. Mini PROTACs: N-end rule-mediated degradation on the horizon. *Trends Biochem. Sci.* **49**, 5–7 (2023).
44. Maple, H. J., Clayden, N., Baron, A., Stacey, C. & Felix, R. Developing degraders: principles and perspectives on design and chemical space. *MedChemComm* **10**, 1755–1764 (2019).
45. Ma, J. et al. iProX: an integrated proteome resource. *Nucleic Acids Res.* **47**, D1211–D1217 (2019).
46. Chen, T. et al. iProX in 2021: connecting proteomics data sharing with big data. *Nucleic Acids Res.* **50**, D1522–D1527 (2022).

Acknowledgements

We are grateful to the members of the Rao lab for discussion and the reagents from Dr. Xianming Deng, Hongbin Ji, Ke Ding, Zhang Zhang, Hong Rui Wang. This study was supported by the National Key Research and Development Program (2021YFA0909300 to H.R.), National Natural Science Foundation of China (82473177 to J.Z. and 82170159 to H.R.), the Natural Science Foundation of Guangdong Province (2025A1515011516 to J.Z. and 2023A1515011765 to L.F.), Shenzhen Fundamental Research Program (JCYJ20220818100412028 to H.R., JCYJ20210324105007019 to J.Z. and JCYJ20220818101404010 to L.F.), Shenzhen Medical Research Funds (B2401008 to L.F.), Key Talent Program of Guangdong (2021CX02Y084 to H.R.), High level of special funds (G03050K003 to H.R.), Medical Research Innovation Project (G030410001 to H.R.), M.-Y.S. is an investigator of SUSTech Institute for Biological Electron Microscopy.

Author contributions

J.Z., L.F., and H.R. designed the experiments. J.Z., C.C., X.C., K.L., F.L., X.S., and C.L. performed the experiments. J.Z., C.C., L.F., F.L., M.-Y.S., H.S., T.H., and C.S.H.T. analyzed data. J.Z. and H.R. wrote the manuscript.

Competing interests

H.R., J.Z., and L.F. are co-inventors on a patent application related to the PROTACs described in this paper (applicant: Southern University of Science and Technology; Shenzhen Institute of Advanced Technology, Chinese Academy of Sciences; inventors: H.R., J.Z., and L.F.; application number: PCT/CN2024/129836). The other authors declare no competing interests.

Additional information

Supplementary information The online version contains supplementary material available at https://doi.org/10.1038/s41467-025-60107-7.

Correspondence and requests for materials should be addressed to Lijing Fang or Hai Rao.

Peer review information *Nature Communications* thanks the anonymous reviewer(s) for their contribution to the peer review of this work. A peer review file is available.